Experimental validation of vehicle velocity, attitude and IMU bias estimation

Available online at www.sciencedirect.com

ScienceDirect

IFAC PapersOnline CONFERENCE PAPER ARCHIVE

IFAC PapersOnLine 52-8 (2019) 118–123

Experimental Validation of Vehicle Velocity, Attitude and IMU Bias Estimation

Wouter J. Scholte * **Vicent Rodrigo Marco** **,*** **Henk Nijmeijer** *

* *Mechanical Engineering Department, Eindhoven University of Technology, Eindhoven, Netherlands (e-mail: w.j.scholte@tue.nl, h.nijmeijer@tue.nl).*
** *Research and Development, Daimler AG, 71059 Sindelfingen, Germany (e-mail: vicent.rodrigo_marco@daimler.com)*
*** *Control Systems Group, Department of Electrical Engineering and Computer Science, Technische Universität Berlin, D-10587 Berlin, Germany*

Abstract: This paper proposes an estimation method for the three dimensional velocity, and the roll and pitch angles of a land vehicle. The usage of low-cost sensors is required for applications in production vehicles. The proposed estimation method uses a low-cost inertial measurement unit (IMU) of which the biases are estimated. A nonlinear system is used to create an observer for simultaneous state and parameter estimation. Experimental results show the potential of this approach in a real world environment.

Keywords: Autonomous vehicles, State estimation, Parameter estimation, Sensor fusion, Inertial measurement units, Motion estimation.

1. INTRODUCTION

Many systems in automated vehicles require information such as the velocity and attitude angles of this vehicle. The direct measurement of these motion states can be performed with advanced equipment. However, such devices are costly and thus unsuitable for implementation in production vehicles. Therefore, estimation methods using the available low-cost sensors are necessary for the realization of affordable automated vehicles.

Vehicle state estimation has long been a subject of investigation in the automotive field. There are multiple approaches to perform these estimations. Many approaches make use of some nonlinear variation of the Kalman Filter, examples can be found in Amirsadri et al. (2012), Collin (2015), Katriniok and Abel (2016), and Vargas-Melendez et al. (2017). The advantage of this approach is that sensor noise can easily be accounted for. However, in nonlinear cases these filters are often not proven to be globally stable. Another approach for vehicle state estimation is the use of nonlinear observers, such as seen in Berkane and Tayebi (2017), and Imsland et al. (2006). These are often proven to be globally stable but are likely to be affected by measurement noise.

Often a Global Navigation Satellite System (GNSS) receiver is used in vehicle motion estimation, examples include Amirsadri et al. (2012), Berkane and Tayebi (2017), Berntorp (2016), Katriniok and Abel (2016), and Zhao et al. (2016). The GNSS is able to provide the vehicle with three dimensional position and velocity. However, in an urban environment GNSS outages may occur affecting the motion estimation.

This work proposes a vehicle motion estimator for land vehicles. The estimator is based on an observer rather than a Kalman Filter such that global convergence can be guaranteed. Furthermore, the longitudinal and lateral accelerometer bias are estimated online. Therefore, the influence of these sensor errors on the performance of the observer is lowered. Direct use of GNSS is avoided such that the estimator is applicable in urban environments. The estimated states are the three dimensional velocity, and the pitch and roll of the vehicle.

The vehicle is equipped with a six degrees of freedom (6DOF) inertial measurement unit (IMU) as well as standard chassis sensors. A 6DOF IMU is a device that can measure three dimensional translational accelerations and rotational velocities. An inexpensive IMU is used, which has relatively large measurement errors. The accuracy is improved by simultaneously estimating the vehicle states and the IMU biases.

The main error sources of the low-cost IMU include non-orthogonalities, non-linearities, scaling factors, biases and noise. Non-orthogonalities describe the relative direction of the accelerometers and gyroscopes inside the IMU. Non-linearities are present in the mapping between the physical signal and sensor output which is assumed linear. Scaling factors are errors in the estimation of the slope of this linear mapping. Biases are offsets in the sensor output that are constant for all physical signals. Due to the integration process in the motion estimator, the error caused by

10.1016/j.ifacol.2019.08.058

uncompensated IMU biases will accumulate. The motion estimation errors caused by the biases are a function of time, as shown in Li et al. (2015). This is unlike the other error sources, such as scaling factors, where the resulting errors are dependent on the excitations. Therefore, biases are often considered as the most significant IMU error source in vehicle motion estimation. It should be noted that biases can slowly change over time due to temperature changes. In this work, the estimation of the lateral and longitudinal accelerometer bias will be performed while driving. Other biases are estimated while standing still.

In the following section, the vehicle motion model on which the observer will be based is given. This includes the modeling of the IMU error parameters. In Section 3 the proposed observer design is presented. Experimental results using real world measurements are shown in Section 4. Lastly, in Section 5 conclusions are drawn and future work is proposed.

2. VEHICLE MOTION MODEL

This section describes the vehicle motion model. A set of ordinary differential equations (ODEs) is used to describe the behavior of the vehicle. The inputs of the ODEs are measured by the IMU. Therefore, the IMU errors must be modeled for practical implementation of this motion model. The IMU error model is described in the second subsection.

2.1 Vehicle model

A kinematic model is used to describe the behavior of the vehicle motion states. The required motion states are the three dimensional velocity, and the roll and pitch angles. First, the derivatives of the three velocities are defined as seen in Klier et al. (2008),

$$\begin{bmatrix}\dot{v}_x\\ \dot{v}_y\\ \dot{v}_z\end{bmatrix} = \begin{bmatrix}a_x^s\\ a_y^s\\ a_z^s\end{bmatrix} - \begin{bmatrix}\omega_x\\ \omega_y\\ \omega_z\end{bmatrix} \times \begin{bmatrix}v_x\\ v_y\\ v_z\end{bmatrix} + \begin{bmatrix}g\sin\theta\\ -g\sin\phi\cos\theta\\ -g\cos\phi\cos\theta\end{bmatrix}. \quad (1)$$

Here v_x, v_y, and v_z are the longitudinal, lateral, and vertical velocity in the body-fixed frame. Furthermore, a_x^s, a_y^s, and a_z^s denote the longitudinal, lateral, and vertical acceleration in the body-fixed frame respectively. The superscript s denotes that a gravitational component is present in these accelerations. Rotational velocities ω_x, ω_y, and ω_z are around the longitudinal, lateral, and vertical axes of the body-fixed frame. Constant g denotes the acceleration of gravity. Lastly, the pitch and roll angles are indicated using θ and ϕ as shown in Figure 1. In this figure x_e, y_e and z_e are the earth fixed axis and x, y and z are the longitudinal, lateral and vertical axis of the vehicle.

Equations to describe the dynamics of θ and ϕ can be found in Wendel (2011), and are

$$\begin{aligned}\dot{\theta} &= \omega_y\cos(\phi) - \omega_z\sin(\phi)\\ \dot{\phi} &= \omega_x + \omega_y\sin(\phi)\tan(\theta) + \omega_z\cos(\phi)\tan(\theta).\end{aligned} \quad (2)$$

Now three states regarding the attitude angles can be defined as $x_4 = \sin(\theta)$, $x_5 = \sin(\phi)\cos(\theta)$ and $x_6 = \cos(\phi)\cos(\theta)$. It should be noted that these states satisfy the constraint $x_4^2 + x_5^2 + x_6^2 = 1$. Using (2) their derivatives yield

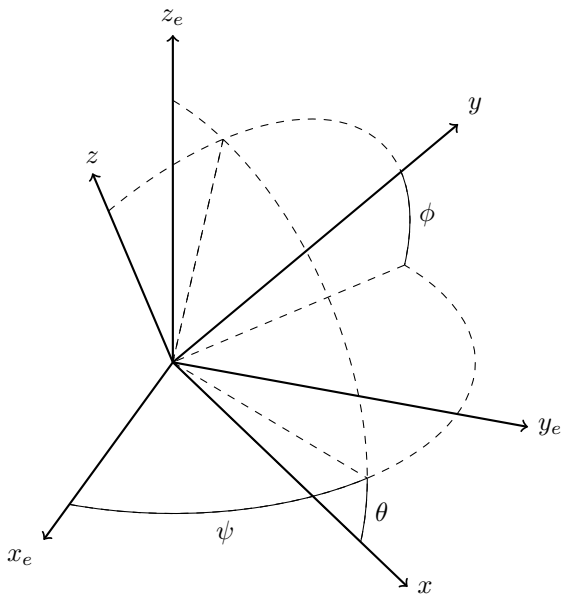

Fig. 1. Definition of the vehicle attitude angles where subscript e denotes earth fixed axis

$$\begin{aligned}\dot{x}_4 &= \cos(\theta)\dot{\theta} = \omega_y\cos(\theta)\cos(\phi) - \omega_z\cos(\theta)\sin(\phi)\\ &= -\omega_z x_5 + \omega_y x_6\\ \dot{x}_5 &= \cos(\theta)\cos(\phi)\dot{\phi} - \sin(\theta)\sin(\phi)\dot{\theta}\\ &= \omega_x\cos(\theta)\cos(\phi) + \omega_z\sin(\theta) = \omega_z x_4 + \omega_x x_6\\ \dot{x}_6 &= -\sin(\theta)\cos(\phi)\dot{\theta} - \cos(\theta)\sin(\phi)\dot{\phi}\\ &= -\omega_x\cos(\theta)\sin(\phi) - \omega_y\sin(\theta) = -\omega_y x_4 - \omega_x x_5.\end{aligned} \quad (3)$$

These derivatives satisfy the previously mentioned constraint as $x_4\dot{x}_4 + x_5\dot{x}_5 + x_6\dot{x}_6 = 0$.

The state vector contains the velocities and attitude angles. The resulting state vector is defined as

$$x = \left[v_x,\ v_y,\ v_z,\ \sin(\theta),\ \sin(\phi)\cos(\theta),\ \cos(\phi)\cos(\theta)\right]^T. \quad (4)$$

Now, (1) and (3) can be combined into a dynamic system such that

$$\begin{aligned}\dot{x}_1 &= u_3x_2 - u_2x_3 + gx_4 + u_4\\ \dot{x}_2 &= -u_3x_1 + u_1x_3 - gx_5 + u_5\\ \dot{x}_3 &= u_2x_1 - u_1x_2 - gx_6 + u_6\\ \dot{x}_4 &= u_2x_6 - u_3x_5\\ \dot{x}_5 &= u_1x_6 + u_3x_4\\ \dot{x}_6 &= -u_2x_4 - u_1x_5.\end{aligned} \quad (5)$$

Where u denotes the input vector

$$u_{1,\dots,6} = \left[\omega_x,\ \omega_y,\ \omega_z,\ a_x^s,\ a_y^s,\ a_z^s\right]^T. \quad (6)$$

An observer design requires an output that can be measured with the available sensors. Using the wheel speeds the longitudinal velocity with respect to the road (v_x^G) can be measured. Furthermore, sensors in the suspension are used to determine the vertical velocity (v_z^G), the pitch (θ^G) and the roll (ϕ^G) with respect to the ground. The velocities with respect to the ground can then be related to the velocities in the vehicle frame using

$$\begin{aligned}v_x^G &= v_x + v_z\theta^G + h_n\dot{\theta}^G\\ v_z^G &= v_z - v_x\theta^G + v_y\phi^G.\end{aligned} \quad (7)$$

Where h_n denotes the distance between the pitch center and center of gravity with respect to the ground.

Next, the lateral velocity is estimated using a classic single track model as shown in Mitschke and Wallentowitz (1972). We assume lateral accelerations below 4 m/s^2 in dry road conditions. Therefore, a linear relation between rear lateral tire force ($F_{y,r}$) and tire side slip angle (α_r) can be assumed. The relation between the angle and force is described as

$$F_{y,r} = c_{\alpha,r}\alpha_r. \tag{8}$$

Where $c_{\alpha,r}$ is the cornering stiffness of the rear tire.

Within the limits of the linear tire approximation (8), α_r is considered to be small. It can be approximated using

$$\alpha_r = \arctan\left(\frac{l_r\omega_z - v\sin\beta}{v\cos\beta}\right) \approx \frac{l_r\omega_z - v_y}{v_x}. \tag{9}$$

Where l_r is the distance from the center of gravity to the rear axle and v is the vehicle speed.

The force and moment equilibria of the single track model are written as

$$m\ a_y^s = F_{y,f} + F_{y,r} \tag{10}$$

$$J_z\dot{\omega}_z = l_f F_{y,f} - l_r F_{y,r}. \tag{11}$$

Where m denotes the vehicle mass and the lateral force on the front tire is denoted by $F_{y,f}$. J_z denotes the moment of inertia around the z axes and l_r is the distance from the center of gravity to the rear axle.

Combining (8), (9), (10) and (11) yields

$$l_f m\ a_y^s - J_z\dot{\omega}_z = (l_f + l_r)c_{\alpha,r}\frac{l_r\omega_z - v_y}{v_x} \tag{12}$$

$$v_y = l_r\omega_z - \frac{l_f\ m}{c_{\alpha,r}l}a_y^s v_x + \frac{J_z\dot{\omega}_z v_x}{c_{\alpha,r}l}. \tag{13}$$

where $l = l_f + l_r$ denotes the total distance between the front and rear axle. For quasi-static lateral dynamics, $\dot{\omega}_z$ is approximately zero. The lateral velocity may then be expressed as

$$v_y \approx l_r\omega_z - SG a_y^s v_x \tag{14}$$

where $SG = \frac{l_f\ m}{c_{\alpha,r}l}$ denotes the side slip angle gradient. This vehicle specific parameter is assumed to be known.

The measurable output vector y and input vector u are now defined as

$$\begin{aligned} y &= \begin{bmatrix} v_x^G - h_n\dot{\theta}^G \\ l_r\omega_z \\ v_z^G \end{bmatrix} = \begin{bmatrix} v_x + v_z\theta^G \\ v_y + a_y^s v_x SG \\ v_z - v_x\theta^G + v_y\phi^G \end{bmatrix} \\ &= \begin{bmatrix} x_1 + x_3u_7 \\ x_2 + x_1u_5SG \\ x_3 - x_1u_7 + x_2u_8 \end{bmatrix}, \end{aligned} \tag{15}$$

$$u_{1,\dots,8} = \begin{bmatrix}\omega_x,\ \omega_y,\ \omega_z,\ a_x^s,\ a_y^s,\ a_z^s,\ \theta^G,\ \phi^G\end{bmatrix}^T. \tag{16}$$

The full system is thus described by (5) and (15). It should be noted that the inputs of this model are subject to physical limitations of the vehicle and cannot be actuated directly. However, the vector u is known because its components are measurable.

2.2 IMU error model

Practical limitations of the previously proposed system will be encountered when a low-cost IMU is used. Measurement errors in u will cause state estimation errors. The most important errors in the IMU are biases, these are constant offsets that will accumulate over time when the signal is integrated. The magnitude of the biases may change when the sensor switched on and off or due to temperature changes.

Rodrigo Marco et al. (2018) shows that the biases in the gyroscopes can be estimated when the vehicle is standing still. The earth rotation is negligible due to the proposed IMU's accuracy. The vertical accelerometer bias ($b_{a,z}$) can be expressed as

$$b_{a,z} = a_{m,z}^s - a_z - \omega_x v_y + \omega_y v_x - g\cos\phi\cos\theta. \tag{17}$$

Here the subscript m denotes that the acceleration is a measurement that includes the bias. Whenever the vehicle is standing still, and ϕ and θ are small enough, $b_{a,z}$ can be estimated using the simplification $b_{a,z} = a_{m,z}^s - g$. Longitudinal and lateral accelerometer biases cannot be estimated similarly because of the unknown influence of g on the measured signal for any ϕ and θ. Therefore, the lateral and longitudinal accelerometer biases must be estimated while driving.

To model the biases, a time invariant parameter vector

$$\rho = [b_{a,x},\ b_{a,y}] \tag{18}$$

is introduced. Here $b_{a,i}$ is the bias of measurement $a_{m,i}^s$. From this point on u_4 and u_5 will be redefined as measurements $a_{m,x}^s$ and $a_{m,y}^s$ respectively. Such that $a_x^s = u_4 - \rho_1$ and $a_y^s = u_5 - \rho_2$.

This changes the dynamics of (5) and the second output equation in (15) to,

$$\begin{aligned} \dot{x}_1 &= u_3x_2 - u_2x_3 + gx_4 + u_4 - \rho_1 \\ \dot{x}_2 &= -u_3x_1 + u_1x_3 - gx_5 + u_5 - \rho_2 \\ \dot{x}_3 &= u_2x_1 - u_1x_2 - gx_6 + u_6 \\ \dot{x}_4 &= u_2x_6 - u_3x_5 \\ \dot{x}_5 &= u_1x_6 + u_3x_4 \\ \dot{x}_6 &= -u_2x_4 - u_1x_5 \end{aligned} \tag{19}$$

and

$$y_2 = x_2 + x_1u_5SG - x_1\rho_2SG. \tag{20}$$

To simplify (20), v_x is approximated by v_x' such that

$$\begin{aligned} v_x &= \frac{v_x^G + h_n\dot{\theta}^G + v_z^G\theta^G + v_y\phi^G\theta^G}{1 + \theta^{G^2}} \\ &\approx \frac{v_x^G + h_n\dot{\theta}^G + v_z^G\theta^G}{1 + \theta^{G^2}} = v_x'. \end{aligned} \tag{21}$$

Since v_x' is measurable, the vehicle model with IMU errors is now described using the state dynamics in (19) and

$$y = \begin{bmatrix} x_1 + x_3u_7 \\ x_2 + x_1u_5SG - \rho_2u_9SG \\ x_3 - x_1u_7 + x_2u_8 \end{bmatrix} \tag{22}$$

$$u = \begin{bmatrix}\omega_x,\ \omega_y,\ \omega_z,\ a_{m,x}^s,\ a_{m,y}^s,\ a_z^s,\ \theta^G,\ \phi^G,\ v_x'\end{bmatrix}^T. \tag{23}$$

2.3 Observability and identifiability analysis

Observability and identifiability are notions in control theory that are important for state and parameter estimation respectively. A system is *locally observable at* x_0 if there exists a neighborhood W around x_0 such that for every neighborhood $V \subset W$ of x_0, an x_1 being V-indistinguishable with x_0 implies that $x_0 = x_1$. A system is *locally observable* if it's *locally observable at any* x_0,

see Nijmeijer and Van der Schaft (1990). The notion of identifiability states that if the known quantities of the system result in a single solution for the parameters the system is *parameter identifiable*. If there is an infinite amount of possible solutions for the parameter the system is *unidentifiable* as stated in Distefano and Cobelli (1980).

Let us now define a smooth affine control system as

$$\begin{aligned} \dot{x} &= f(x) + \sum_{j=1}^{m} g_j(x)u_j, \quad u = (u_1, \ldots, u_m), \\ y_i &= h_i(x), \quad i \in p. \end{aligned} \tag{24}$$

Where x are local coordinates on a smooth manifold M and $f, g_1, \ldots, g_m$ are smooth vectorfields on M. m and p are the number of inputs and outputs respectively. The observation space $\mathscr{O}$ is defined as the linear space of functions on M containing $h_1, \ldots, h_p$ and all of its Lie derivatives. The observability codistribution ($d\mathscr{O}$) is defined as $d\mathscr{O}(q) = \text{span}\{dH(q) | H \in \mathscr{O}\}$ for $q \in M$. In Nijmeijer and Van der Schaft (1990) it's shown that if $\dim d\mathscr{O}(x_0) = \dim M$ then the system is locally observable at x_0. If state vector x is extended with parameters modeled as states with zero time derivative, local identifiability can be shown using this method.

This system is locally observable for all inputs u. However, the local identifiability is dependent on input u. In general it can be said that the parameters are identifiable when ω_z is nonzero. More information regarding observability and identifiability of this system can be found in Rodrigo Marco et al. (2018).

3. ESTIMATOR DESIGN

The vehicle model with IMU errors of section 2.2 can be written as a linear time varying (LTV) system. The system is of the form

$$\begin{aligned} \dot{x}(t) &= A(u(t))x(t) + Bu(t) + \Psi\rho \\ y(t) &= C(u(t))x(t) + \Omega(u(t))\rho. \end{aligned} \tag{25}$$

Matrices dependent on a time varying input $u(t)$ can be seen as matrices dependent on the time.

3.1 State and parameter estimation

For systems of the form (25) a combination of the observers from Li et al. (2011), and Hammouri and de Leon Morales (1990) can be used. This combined observer is as follows,

$$\begin{aligned} \dot{\hat{x}}(t) &= A(u(t))\hat{x}(t) + Bu(t) + \Psi\hat{\rho}(t) + K(t)\left[y(t) - \hat{y}(t)\right] \\ &\quad + \Upsilon(t)\Gamma\left[C(u(t))\Upsilon(t) + \Omega(u(t))\right]^T \Sigma\left[y(t) - \hat{y}(t)\right] \\ \hat{y}(t) &= C(u(t))\hat{x}(t) + \Omega(u(t))\hat{\rho}(t) \\ \dot{\hat{\rho}}(t) &= \Gamma\left[C(u(t))\Upsilon(t) + \Omega(u(t))\right]^T \Sigma\left[y(t) - \hat{y}(t)\right] \\ \dot{\Upsilon}(t) &= \left[A(u(t)) - K(t)C(u(t))\right]\Upsilon(t) + \Psi - K(t)\Omega(u(t)) \\ \Upsilon(0) &= 0 \\ K(t) &= R^{-1}(t)C^T(t) \\ \dot{R}(t) &= -\lambda R(t) - A^T(u(t))R(t) - R(t)A(u(t)) \\ &\quad + C^T(u(t))C(u(t)) \\ R(0) &= R^T(0) > 0. \end{aligned} \tag{26}$$

Where $\hat{x}$, $\hat{y}$ and $\hat{\rho}$ are state, output and parameter estimates. The matrices $A(u(t))$, B, $C(u(t))$, Ψ and $\Omega(u(t))$ are obtained from (25). The symmetric positive definite 2×2 matrix Γ, 3×3 matrix Σ, and scalar $\lambda > 0$ can be used to tune the observer. It should be noted that Σ can scale the influence of the different outputs on the estimates. This could take the expected accuracy of the measurements into consideration. Gain matrices $\Upsilon(t)$, $K(t)$ and $R(t)$ are governed by (26).

3.2 Stability analysis

The work of Hammouri and de Leon Morales (1990) shows that the dynamics of $R(t)$ (and thus $K(t)$) are such that the system

$$\dot{\eta}(t) = [A(u(t)) - K(t)C(u(t))]\eta(t) \tag{27}$$

is exponentially stable. It should be noted that this holds because our system is observable for all inputs.

We now define state error $\tilde{x}(t) = \hat{x}(t) - x(t)$ and parameter error $\tilde{\rho}(t) = \hat{\rho}(t) - \rho$. Using the works of Li et al. (2011) and Zhang (2002) it can then be shown that $\tilde{x}(t) \to \Upsilon(t)\tilde{\rho}(t)$ with global and exponential convergence. Furthermore, $\tilde{\rho}(t)$ is stable under all inputs and exponentially stable when the system is identifiable. In essence, our states are estimated with an error based on our parameter estimation error. Estimate $\hat{\rho}(t)$ will only converge to ρ when the system is identifiable and remain constant when the system is unidentifiable. Since $\Upsilon(t)$ is bounded it can be concluded that if $\tilde{\rho}(t) \to 0$ then $\tilde{x}(t) \to 0$.

4. EXPERIMENTAL RESULTS

To obtain experimental results a measurement has been performed in an urban environment. This section first describes the experiment, then the experimental results are discussed.

4.1 Experimental setup and measurement

To perform the experiment the vehicle was equipped with a high precision inertial navigation system (INS) and differential GNSS (DGNSS) combination. This system is too costly to implement in a production vehicle but was used to compute the errors of the estimates. The measured states are shown in Figures 2 and 3. Furthermore, rotational velocity ω_z is shown in Figure 4, this gives an indication of the identifiability. In Figure 5 it is shown that the lateral acceleration is below 4 m/s^2 for almost the entire measurement. Therefore, the assumptions for the vehicle model are satisfied.

The observer parameters have been tuned and are $\Gamma = 0.05I$, $\lambda = 0.35$, and $\Sigma = I$. Furthermore, the side slip angle gradient SG was estimated to be 0.00683. Lastly, the initial values of R, and the state and parameter estimates were chosen to be $R(0) = I$, $\hat{x}(0) = [0\ 0\ 0\ 0\ 0\ 1]^T$ and $\hat{\rho}(0) = [0\ 0]^T$. The input data was measured at 100 Hz and a differential solver (*ode45*) in MATLAB was used to solve (26).

4.2 Estimated states and parameters

The errors in the velocity estimation are shown in Figure 6 where error $\tilde{v}_i = \hat{v}_i - v_i$ and $\hat{v}$ is the estimated velocity.

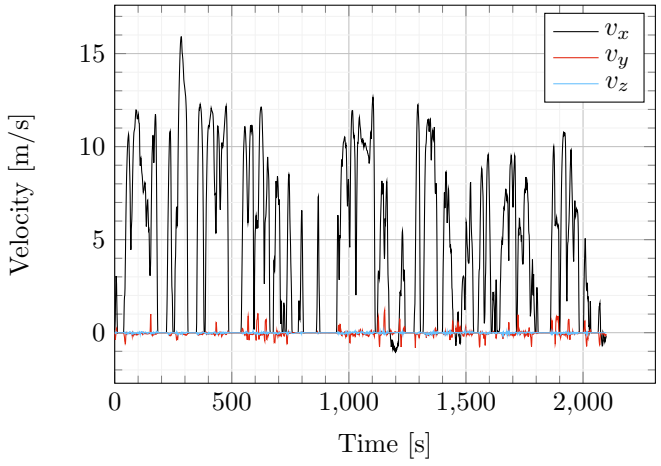

Fig. 2. Velocities v_x, v_y and v_z from the reference signal.

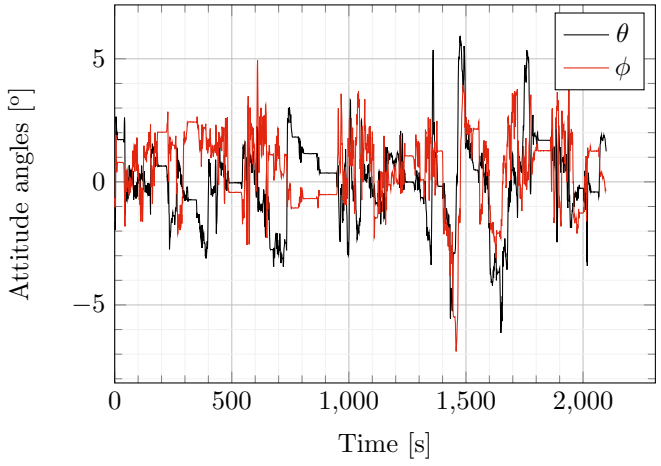

Fig. 3. Angles θ and ϕ from the reference signal.

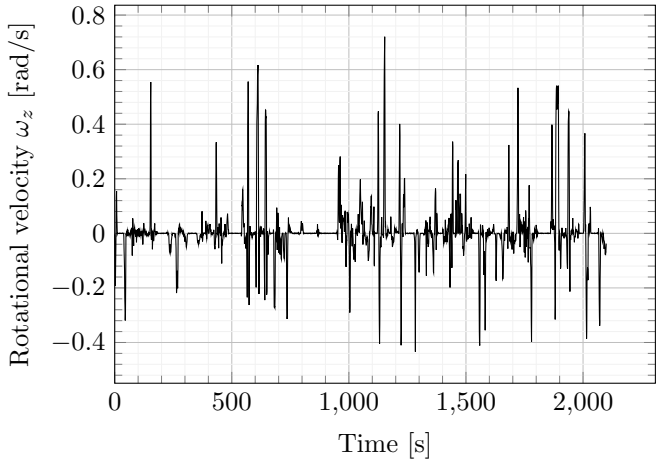

Fig. 4. Rotational velocity ω_z from the reference signal.

The amplitude of these errors remains relatively constant over time with a mean value around 0.

The errors in the attitude angle estimation are shown in Figure 7 where $\tilde{\theta}$ and $\tilde{\phi}$ are defined similar to $\tilde{v}$. It can be seen that the attitude angles have an offset at the start of the measurement. At the end of the measurement, the errors have a mean value much closer to 0. The remaining

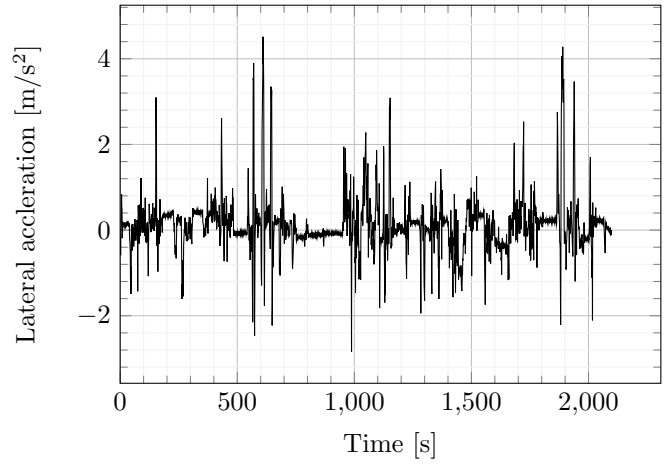

Fig. 5. Lateral acceleration a_y from the reference signal.

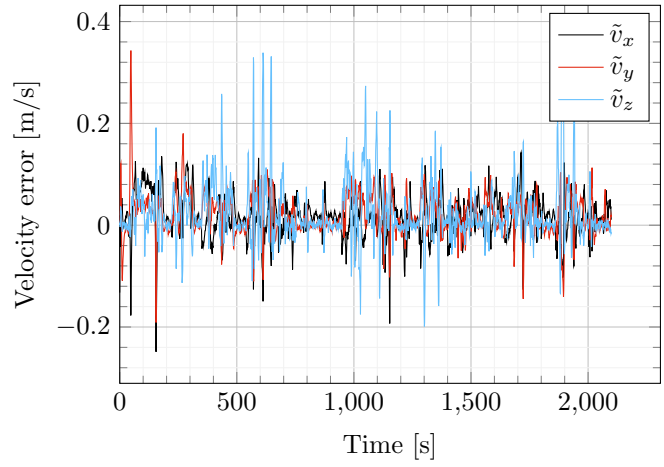

Fig. 6. Estimation errors $\tilde{v}_x$, $\tilde{v}_y$ and $\tilde{v}_z$.

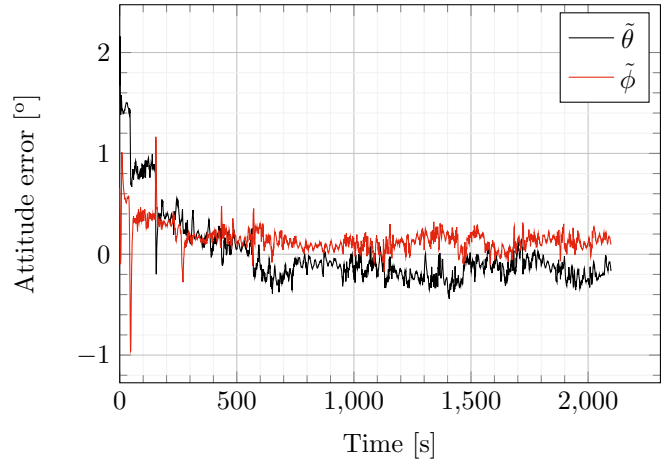

Fig. 7. Estimation errors $\tilde{\theta}$ and $\tilde{\phi}$.

offset is likely due to some unmodeled errors. The behavior of this offset can be explained using the accelerometer bias estimation shown in Figure 8. At the start of the measurement, the bias estimations have not yet converged, causing an error in the attitude angle estimation. As the bias estimates get close to their true values, the attitude angle estimation becomes more precise.

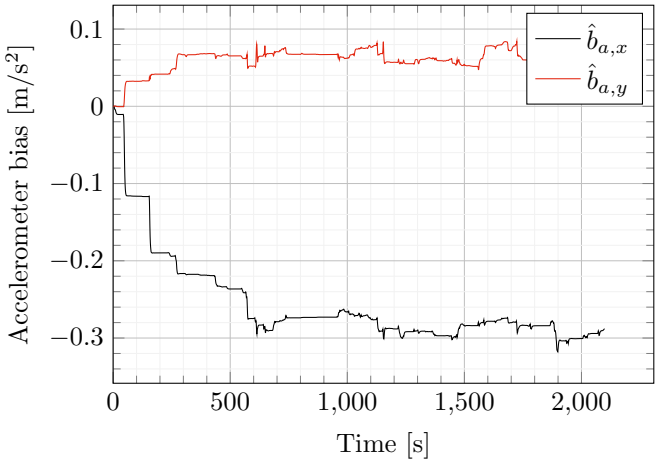

Fig. 8. Accelerometer bias estimates $\hat{b}_{a,x}$ and $\hat{b}_{a,y}$.

From the previous graphs, it can be concluded that the velocity estimation is relatively unaffected by the parameter estimation. The estimated attitude angles show the need for an accurate accelerometer bias estimation. The uncompensated biases are interpreted as a gravitational component due to an attitude angle. The magnitude of $\tilde{\theta}$ and $\tilde{\phi}$ in the second part of the measurement suggests that the IMU biases are estimated correctly.

Figure 4 and Figure 8 demonstrate the effect of input ω_z on the estimates $\hat{\rho}$. The estimated parameters remain constant for certain periods of time during which the ω_z is close to zero. The model is not identifiable but the parameter estimation remains stable. When the system experiences excitations of ω_z the model is identifiable and estimate $\hat{\rho}$ converges to parameter value ρ.

5. CONCLUSIONS

Prior work in vehicle motion estimation is often based on some Kalman Filter that cannot be proven globally stable. Observer based estimators often use GNSS receivers (Berkane and Tayebi (2017)) or neglect measurement errors (Imsland et al. (2006)). This work aims at an estimator that includes the IMU biases to limit the effect of measurement errors.

An observer based estimator that estimates the accelerometer biases online is proposed. The usage of a GNSS receiver was avoided to ensure that GNSS errors in an urban environment do not affect the estimator's performance. The observer is proven to be globally stable. Experiments show the potential of this approach in urban environments. Future research may aim at adding additional data from other sensors when available.

REFERENCES

Amirsadri, A., Kim, J., Petersson, L., and Trumpf, J. (2012). Practical considerations in precise calibration of a low-cost mems imu for road-mapping applications. In *American Control Conference (ACC), 2012*, 881–888. IEEE.

Berkane, S. and Tayebi, A. (2017). Attitude and gyro bias estimation using gps and imu measurements. In *Decision and Control (CDC), 2017 IEEE 56th Annual Conference on*, 2402–2407. IEEE.

Berntorp, K. (2016). Joint wheel-slip and vehicle-motion estimation based on inertial, gps, and wheel-speed sensors. *IEEE Transactions on Control Systems Technology*, 24(3), 1020–1027.

Collin, J. (2015). Mems imu carouseling for ground vehicles. *IEEE Transactions on Vehicular Technology*, 64(6), 2242–2251.

Distefano, J. and Cobelli, C. (1980). On parameter and structural identifiability: Nonunique observability/reconstructibility for identifiable systems, other ambiguities, and new definitions. *IEEE Transactions on Automatic Control*, 25(4), 830–833.

Hammouri, H. and de Leon Morales, J. (1990). Observer synthesis for state-affine systems. In *Decision and Control, 1990., Proceedings of the 29th IEEE Conference on*, 784–785. IEEE.

Imsland, L., Johansen, T.A., Fossen, T.I., Grip, H.F., Kalkkuhl, J.C., and Suissa, A. (2006). Vehicle velocity estimation using nonlinear observers. *Automatica*, 42(12), 2091–2103.

Katriniok, A. and Abel, D. (2016). Adaptive ekf-based vehicle state estimation with online assessment of local observability. *IEEE Transactions on Control Systems Technology*, 24(4), 1368–1381.

Klier, W., Reim, A., and Stapel, D. (2008). Robust estimation of vehicle sideslip angle-an approach w/o vehicle and tire models. Technical report, SAE Technical Paper.

Li, X., Zhang, Q., and Su, H. (2011). An adaptive observer for joint estimation of states and parameters in both state and output equations. *International Journal of adaptive control and signal processing*, 25(9), 831–842.

Li, Y., Zhang, P., Niu, X., Zhuang, Y., Lan, H., and El-Sheimy, N. (2015). Real-time indoor navigation using smartphone sensors. In *2015 International Conference on Indoor Positioning and Indoor Navigation (IPIN)*, 1–10.

Mitschke, M. and Wallentowitz, H. (1972). *Dynamik der kraftfahrzeuge*, volume 4. Springer.

Nijmeijer, H. and Van der Schaft, A. (1990). *Nonlinear dynamical control systems*, volume 175. Springer.

Rodrigo Marco, V., Kalkkuhl, J., and Raisch, J. (2018). Ekf for simultaneous vehicle motion estimation and imu bias calibration with observability-based adaptation. In *2018 Annual American Control Conference (ACC)*, 6309–6316. IEEE.

Vargas-Melendez, L., Boada, B.L., Boada, M.J.L., Gauchia, A., and Diaz, V. (2017). Sensor fusion based on an integrated neural network and probability density function (pdf) dual kalman filter for on-line estimation of vehicle parameters and states. *Sensors*, 17(5), 987.

Wendel, J. (2011). *Integrierte Navigationssysteme: Sensordatenfusion, GPS und Inertiale Navigation*. Walter de Gruyter.

Zhang, Q. (2002). Adaptive observer for multiple-input-multiple-output (mimo) linear time-varying systems. *IEEE transactions on automatic control*, 47(3), 525–529.

Zhao, S., Chen, Y., and Farrell, J.A. (2016). High-precision vehicle navigation in urban environments using an mem's imu and single-frequency gps receiver. *IEEE transactions on intelligent transportation systems*, 17(10), 2854–2867.